Journal of Advances in Mathematics and Computer Science

33(1): 1-15, 2019; Article no.JAMCS.48578

ISSN: 2456-9968

(Past name: British Journal of Mathematics & Computer Science, Past ISSN: 2231-0851)

Cramér-Rao Bound of Direction Finding Using Uniform Arc Arrays

Veronicah Nyokabi[1*], Dominic Makaa Kitavi[1] and Cyrus Gitonga Ngari[1]

[1] *Department of Mathematics, Computing and Information Technology, University of Embu, Kenya.*

Authors' contributions

This work was carried out in collaboration Among all authors. Author A designed the study, performed the statistical analysis, wrote the protocol, and wrote the first draft of the manuscript. Author B and Author C managed the analyses of the study. Author C managed the literature searches. All authors read and approved the final manuscript.

Article Information

DOI: 10.9734/JAMCS/2019/v33i130168

Editor(s):

(1) Dr. Burcu Gurbuz, Asssistant Professor, Department of Computer Engineering, Faculty of Engineering and Natural Sciences, Uskudar University, Istanbul, Turkey.

Reviewers:

(1) Boyan Karapenev, Technical University of Gabrovo, Bulgaria.

(2) Christian Parigger, Univ. of TN, USA.

Complete Peer review History: http://www.sdiarticle3.com/review-history/48578

Original Research Article

Received: 10 February 2019

Accepted: 15 April 2019

Published: 13 July 2019

Abstract

Direction-of-Arrival estimation accuracy using arc array geometry is considered in this paper. There is a scanty use of Uniform Arc Array (UAA) in conjunction with Cramér-Rao bound (CRB) for Direction-of-Arrival estimation. This paper proposed to use Uniform Arc Array formed from a considered Uniform Circular Array (UCA) in conjunction with CRB for Direction-of-Arrival estimation. This Uniform Arc Array is obtained by squeezing all sensors on the Uniform Circular Array circumference uniformly onto the Arc Array. Cramér-Rao bounds for the Uniform Arc Array and that of the Uniform Circular Array are derived. Comparison of performance of the Uniform Circular Array and Uniform Arc Array is done. It was observed that Uniform Arc Array has better estimation accuracy as compared to Uniform Circular Array when number of sensors equals four and five and azimuth angle ranging between $\frac{\pi}{9}$ and $\frac{7}{18}\pi$ and also $\frac{10}{9}\pi$ and $\frac{25}{18}\pi$. However, UCA and UAA have equal performance when the number of sensors equals three and

**Corresponding author: E-mail: nyokabiveronicahn@gmail.com;*

the azimuth angle ranging between 0 and 2π. UCA has better estimation accuracy as compared to UAA when the number of sensors equals four and five and the azimuth angle ranging between $\frac{\pi}{2}$ and π and also $\frac{3}{2}\pi$ and 2π.

Keywords: Array signal processing; direction-of-arrival estimation; direction finding; Cramér-Rao bound; uniform arc array.

2010 Mathematics Subject Classification: 53C25; 83C05; 57N16.

1 Introduction

The general performance of any Direction Finding (DF) system is a function of both the DF algorithm used and array geometry [1]. Direction-of-Arrival (DOA)/Direction Finding (DF) is the direction in which an incoming signal arrives into an array of sensors (a group of sensors arranged/organized in a particular pattern). Direction-of-arrival (DOA) estimation is a fundamental problem in array signal processing. Various algorithms have been proposed for DOA estimation such as Multiple Signal Classification (MUSIC), Root-MUSIC, propagator methods, high-order cumulant method, Maximum Likelihood Method (MLM), among many others [2]. Its accuracy is an important parameter of any direction finding system [3]. Cramér-Rao bound is a very important tool for evaluating the accuracy of any parameter estimation method since it provides a lower bound on the accuracy of any unbiased estimator [3]. Performance of various estimators (MUSIC, MLE, among others) is compared to the ultimate performance corresponding to CRB [4]. Regardless of the specific algorithm used, CRB lower bounds estimation error variance of any unbiased estimator [5]. Therefore, CRB provides an algorithm-independent basis against which various algorithms are compared [3]. It has been used in several works such as Cramér-Rao bound for DF using an L-Shaped Array with Non-orthogonal Axes [6], accuracy limits through Cramér-Rao Lower Bound for Geolocation of Internet hosts [7], among many others. One of the simplest array geometry which enables signal array-processing algorithms to be applied easily is the uniform linear array (ULA) [8]. It has useful properties such as application of forward-backward spatial smoothing to only ULA because of the Vandermonde structure of the array steering matrix, application of fast subspace algorithms such as Root-MUSIC in ULA, hence computational efficiency increment [9]. However, ULA will limit azimuth field of view below π (normally $\frac{2}{3}\pi$) since it is one-dimensional. The solution to this problem requires the use of several ULAs arranged in triangular or rectangular shape among others or rotating the ULA a few times to cover the entire azimuth spread. This use of several ULAs increases the cost as well as collecting a lot of data [10]. There are other geometries that have been employed to resolve the problem of the non-uniform performance of ULA in all directions which degrades Direction-of-Arrival (DOA) estimation performance in angles close to endfire [11]. In 2-dimension angle estimation, Uniform Circular Array (UCA) which is a geometrical pattern with a number of sensors equally spaced on the circumference of a circle is highly used due to its attractive advantages such as it provides a 2π full azimuth coverage, has an extra information on elevation angle and its direction pattern is almost unchanged [12]. However, UCA is expected to suffer serious mutual coupling effects because of the compelling coupling that can occur between elements that are positioned diametrically opposite one another together with the strong coupling between adjacent elements. This effect can be compensated since the symmetry of the UCA can break down into a series of symmetrical spatial components using the array excitation [8]. There are different array configurations/geometries in the literature used for DF such as linear, planar and conformal arrays [13]. Unfortunately, very little is known about the arrangement of sensors along a curve or an arc [14]. An arc is a portion or a part of the circumference of a circle. A uniform arc array is a geometrical pattern with a number of sensors equally spaced on an arc. Circular arcs were treated as very important features in the field of pattern recognition such as they were used for

recognizing curved objects. They were also used as shape features for recognition purpose and closed circular arcs were used as local features in identifying and locating partially occluded objects [15]. There is a scanty use of uniform arc array geometry for DOA estimation and therefore this paper proposed to form a uniform arc array (UAA) out of a uniform circular array to be considered for DOA estimation. This paper proposed to use a UCA with a known finite isotropic/identical number of sensors with a narrow-band far-field signal emitted by a single source arriving on the UCA. It is organized as follows; In Section 2 the array geometries (UCA and UAA) will be developed. In section 3 a statistical data model for the geometries will be assumed. In section 4 the CRB of the suggested geometries will be derived. Section 5 will be analysis and section 7 will be the conclusion.

2 Development of the Array Geometries

2.1 Uniform Circular Array

A uniform circular array (UCA) with L number of isotropic sensors equally spaced on the circumference of the circle of radius R, at points S_1 to S_L is considered. These sensors will be considered to be arranged anticlockwise from the positive x-axis where the direction of arrangement does not matter since the sensors are identical. The Cartesian coordinate system origin is assumed to be the central point of the UCA array denoted as O. This point is considered as the reference point. A plane-wave signal from a far-field source is assumed to arrive on O at an azimuth angle ϕ measured anticlockwise from the positive x-axis, and a polar angle θ measured clockwise from the positive z-axis. See Figure 2.1. The position vector for the ℓ^{th} sensor on the UCA, $\mathbf{p}_\ell$, is given by [16]

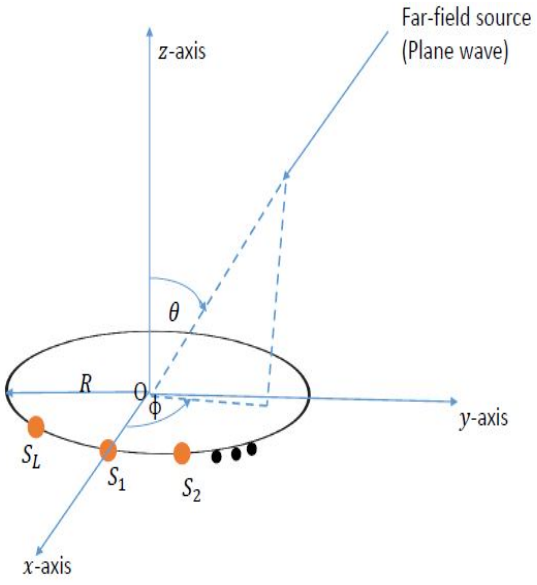

Fig. 1. Uniform Circular Array (UCA).

$$\mathbf{p}_\ell = \left[R\cos\left(\tfrac{2\pi(\ell-1)}{L}\right), R\sin\left(\tfrac{2\pi(\ell-1)}{L}\right), 0\right]^T \tag{2.1}$$

and the array manifold vector for the UCA is

$$\mathbf{a}_{\text{UCA}} = \begin{bmatrix} \exp\left\{i\frac{2\pi R}{\lambda}\sin(\theta)\cos(\phi)\right\} \\ \exp\left\{i\frac{2\pi R}{\lambda}\sin(\theta)\cos(\phi-\frac{2\pi}{L})\right\} \\ \exp\left\{i\frac{2\pi R}{\lambda}\sin(\theta)\cos(\phi-\frac{4\pi}{L})\right\} \\ \vdots \\ \exp\left\{i\frac{2\pi R}{\lambda}\sin(\theta)\cos\left(\phi-\frac{2\pi(L-1)}{L}\right)\right\} \end{bmatrix}. \tag{2.2}$$

2.2 Uniform Arc Array

A uniform arc array (UAA) from the UCA formed by squeezing all L number of sensors onto an arc of a known angle is considered. The sensors are arranged anticlockwise from the positive x-axis. See Figure 2.2. The position vector for the ℓ^{th} sensor on the UAA, $\mathbf{p}_\ell$, is given by

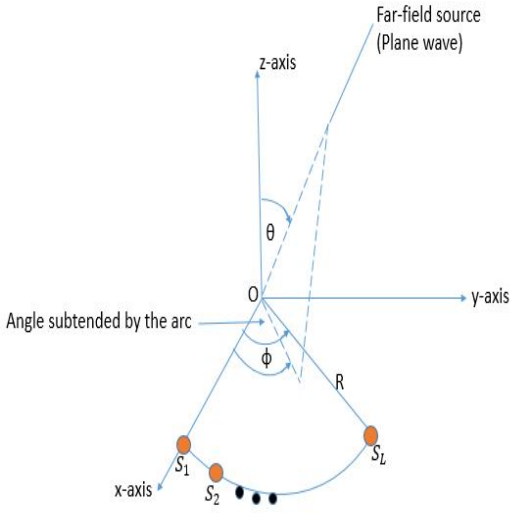

Fig. 2. Uniform Arc Array (UAA).

$$\mathbf{p}_\ell = \left[R\cos\left(\frac{2\pi(\ell-1)}{L(L-1)}\right), R\sin\left(\frac{2\pi(\ell-1)}{L(L-1)}\right), 0\right]^T \tag{2.3}$$

and the corresponding array manifold vector is given by

$$\mathbf{a}_{\text{UAA}} = \begin{bmatrix} \exp\left\{i\frac{2\pi R}{\lambda}\sin(\theta)\cos(\phi)\right\} \\ \exp\left\{i\frac{2\pi R}{\lambda}\sin(\theta)\cos\left(\phi-\frac{2\pi}{L(L-1)}\right)\right\} \\ \exp\left\{i\frac{2\pi R}{\lambda}\sin(\theta)\cos\left(\phi-\frac{4\pi}{L(L-1)}\right)\right\} \\ \vdots \\ \exp\left\{i\frac{2\pi R}{\lambda}\sin(\theta)\cos\left(\phi-\frac{2\pi}{L}\right)\right\} \end{bmatrix}. \tag{2.4}$$

3 Statistical Data Model

Signals impinging on the array of sensors from a certain source are affected/corrupted by additive noise. Thus, at the array of sensors, the observed data for the geometry used is given by [6]

$$\mathbf{z}(m) \quad = \quad \mathbf{a}(\theta,\phi)s(m)+\mathbf{n}(m),\ m=1,2,...,M; \tag{3.1}$$

where $s(m)$ is the signal received at m^{th} time instant and $\boldsymbol{n}(m)$ is the additive noise. From the model, $\boldsymbol{n}(m)$, $\boldsymbol{z}(m)$ and $\mathbf{a}(\theta,\phi)$ will be $L\times 1$ vectors. For multiple time instants/snapshots M, the data model vector will be given by [6]

$$\tilde{\mathbf{z}} \quad = \quad \mathbf{s}\otimes\mathbf{a}(\theta,\phi)+\tilde{\mathbf{n}} \tag{3.2}$$

where

$$\begin{aligned}\tilde{\mathbf{z}} &= [\mathbf{z}(1),\mathbf{z}(2),\cdots,\mathbf{z}(M)]^T,\\ \mathbf{s} &= [s(1),s(2),\cdots,s(M)]^T,\\ \tilde{\mathbf{n}} &= [\mathbf{n}(1),\mathbf{n}(2),\cdots,\mathbf{n}(M)]^T,\end{aligned}$$

and $\otimes$ is the Kronecker product. For simplicity, a pure-tone incident signal $s(m)=\sigma_{_s}\exp[j(2\pi fm+\varphi)]$ will be considered, where $\sigma_{_s}$ is the signals' amplitude and φ is the phase angle. The random variables $\mathbf{z}(1),\mathbf{z}(2),\cdots,\mathbf{z}(M)$ are assumed to be independent and have the same probability distribution. Therefore, the random variable $\tilde{\mathbf{z}}$ has a mean of $\boldsymbol{\mu}(\theta,\phi)$ and a covariance matrix of $\boldsymbol{\Gamma}(\theta,\phi)$ hence it follows a normal distribution $\mathbf{z}\sim\mathcal{N}(\boldsymbol{\mu},\boldsymbol{\Gamma})$ which has a probability density function (likelihood function) $p(\tilde{\mathbf{z}}|\Theta)$ where $\Theta=\{\theta,\phi\}$, i.e.

$$p(\tilde{\mathbf{z}}|\Theta) \ = \ \frac{1}{\sqrt{|2\pi\boldsymbol{\Gamma}|}}\exp\left\{-\frac{1}{2}[\tilde{\mathbf{z}}-\boldsymbol{\mu}]^H\boldsymbol{\Gamma}^{-1}[\tilde{\mathbf{z}}-\boldsymbol{\mu}]\right\}. \tag{3.3}$$

In the above, $\boldsymbol{\mu}=E[\tilde{\mathbf{z}}]$, $\boldsymbol{\Gamma}=E\left\{[\tilde{\mathbf{z}}-\boldsymbol{\mu}][\tilde{\mathbf{z}}-\boldsymbol{\mu}]^H\right\}$ and $|\cdot|$ denotes the corresponding matrix determinant.

$$\begin{aligned}\boldsymbol{\mu} &= E[\tilde{\mathbf{z}}]=E[\boldsymbol{s}\otimes\mathbf{a}(\theta,\phi)+n]\\ &= E[\mathbf{s}\otimes\mathbf{a}(\theta,\phi)]+E[\tilde{\mathbf{n}}]\\ &= \mathbf{s}\otimes\mathbf{a}(\theta,\phi)\end{aligned} \tag{3.4}$$

and

$$\begin{aligned}\boldsymbol{\Gamma} &= E\left\{[\tilde{\mathbf{z}}-\boldsymbol{\mu}][\tilde{\mathbf{z}}-\boldsymbol{\mu}]^H\right\}\\ &= E[\tilde{\mathbf{n}}\tilde{\mathbf{n}}^H]\\ &= \sigma_n^2\mathbf{I}_{ML\times ML}.\end{aligned} \tag{3.5}$$

4 Derivation of the Cramér-Rao Bound

To get the Cramér-Rao bound, the inverse of the Fisher Information Matrix (FIM) is obtained. Since the observed data vector, in this case, is complex-valued, a simplified FIM for multivariate normal distribution is given by [6]

$$\begin{aligned}[\mathbf{F}(\boldsymbol{\xi})]_{k,r} &= 2\mathrm{Re}\left\{\left[\frac{\partial\boldsymbol{\mu}}{\partial\boldsymbol{\xi}_k}\right]^H\boldsymbol{\Gamma}^{-1}\frac{\partial\boldsymbol{\mu}}{\partial\boldsymbol{\xi}_r}\right\}\\ &\quad +\mathrm{Tr}\left\{\boldsymbol{\Gamma}^{-1}\frac{\partial\boldsymbol{\Gamma}}{\partial\boldsymbol{\xi}_k}\boldsymbol{\Gamma}^{-1}\frac{\partial\boldsymbol{\Gamma}}{\partial\boldsymbol{\xi}_r}\right\}.\end{aligned} \tag{4.1}$$

In the above, $\mathrm{Re}\{\cdot\}$ indicates the real part of the identity inside the curly brackets, $\boldsymbol{\xi}=[\theta,\phi]$ is the set of unknown parameters and $k,r=\{1,2\}$.

4.1 Cramér-Rao Bound for the Uniform Circular Array

The FIM here will be given by [6]

$$\mathbf{F}(\boldsymbol{\xi}) = \begin{bmatrix} [\mathbf{F}(\boldsymbol{\xi})]_{1,1} & [\mathbf{F}(\boldsymbol{\xi})]_{1,2} \\ [\mathbf{F}(\boldsymbol{\xi})]_{2,1} & [\mathbf{F}(\boldsymbol{\xi})]_{2,2} \end{bmatrix} \tag{4.2}$$

and therefore computing the entries of the FIM one by one we have, Using (2.2), (3.4) and (3.5) in (4.1), we have

$$[\mathbf{F}(\boldsymbol{\xi})]_{1,1} = ML\left(\frac{2\pi R\sigma_s}{\lambda\sigma_n}\right)^2 \cos^2(\theta), \tag{4.3}$$

$$[\mathbf{F}(\boldsymbol{\xi})]_{2,2} = ML\left(\frac{2\pi R\sigma_s}{\lambda\sigma_n}\right)^2 \sin^2(\theta), \tag{4.4}$$

$$\begin{aligned} [\mathbf{F}(\boldsymbol{\xi})]_{1,2} &= [\mathbf{F}(\boldsymbol{\xi})]_{2,1} \\ &= 0. \end{aligned} \tag{4.5}$$

Thus,

$$\mathbf{F}(\boldsymbol{\xi}) = ML\left(\frac{2\pi R\sigma_s}{\lambda\sigma_n}\right)^2 \begin{bmatrix} \cos^2(\theta) & 0 \\ 0 & \sin^2(\theta) \end{bmatrix}. \tag{4.6}$$

Hence, Cramér-Rao bounds for the UCA are

$$\mathrm{CRB}_{\mathrm{UCA}}(\theta) = \frac{1}{ML}\left(\frac{\lambda\sigma_n}{2\pi R\sigma_s}\right)^2 \sec^2\theta \tag{4.7}$$

and

$$\mathrm{CRB}_{\mathrm{UCA}}(\phi) = \frac{1}{ML}\left(\frac{\lambda\sigma_n}{2\pi R\sigma_s}\right)^2 \csc^2\theta. \tag{4.8}$$

4.2 Cramér-Rao Bound for the Uniform Arc Array

Using (2.4), (3.4) and (3.5) in (4.1), we have

$$[\mathbf{F}(\boldsymbol{\xi})]_{1,1} = 8M\left\{\frac{\pi R\sigma_s}{\lambda\sigma_n}\right\}^2 \left\{\frac{L}{2} + D\right\} \cos^2(\theta), \tag{4.9}$$

$$\begin{aligned} [\mathbf{F}(\boldsymbol{\xi})]_{1,2} &= [\mathbf{F}(\boldsymbol{\xi})]_{2,1} \\ &= -8M\left\{\frac{\pi R\sigma_s}{\lambda\sigma_n}\right\}^2 \{F\} \sin(\theta)\cos(\theta), \end{aligned} \tag{4.10}$$

$$[\mathbf{F}(\boldsymbol{\xi})]_{2,2} = 8M\left\{\frac{\pi R\sigma_s}{\lambda\sigma_n}\right\}^2 \left\{\frac{L}{2} - E\right\} \sin^2(\theta), \tag{4.11}$$

where

$$D = \frac{\sin\left(\frac{2\pi}{L-1}\right)\cos\left(\frac{2\pi}{L} - 2\phi\right)}{2\sin\left(\frac{2\pi}{L(L-1)}\right)},$$

$$E = \frac{\sin\left(\frac{2\pi}{L-1}\right)\cos\left(\frac{2\pi}{L}+2\phi\right)}{2\sin\left(\frac{2\pi}{L(L-1)}\right)},$$

$$F = \frac{-\sin\left(\frac{2\pi}{L-1}\right)\sin\left(-\frac{2\pi}{L}+2\phi\right)}{2\sin\left(\frac{2\pi}{L(L-1)}\right)}.$$

The Cramér-Rao bounds become

$$\mathrm{CRB}_{\mathrm{UAA}}(\theta) = \frac{\lambda^2\sigma_n^2\sec^2(\theta)\gamma}{8\pi^2MR^2\sigma_s^2\beta} \tag{4.12}$$

and

$$\mathrm{CRB}_{\mathrm{UAA}}(\phi) = \frac{\lambda^2\sigma_n^2\csc^2(\theta)\alpha}{8\pi^2MR^2\sigma_s^2\beta} \tag{4.13}$$

where

$$\begin{aligned}\gamma &= \frac{L}{2}-E,\\ &= \frac{L-\sin\left(\frac{2\pi}{L-1}\right)\csc\left(\frac{2\pi}{L(L-1)}\right)\cos\left(\frac{2\pi}{L}+2\phi\right)}{2},\end{aligned} \tag{4.14}$$

$$\begin{aligned}\alpha &= \frac{L}{2}+D,\\ &= \frac{L+\sin\left(\frac{2\pi}{L-1}\right)\csc\left(\frac{2\pi}{L(L-1)}\right)\cos\left(\frac{2\pi}{L}-2\phi\right)}{2},\end{aligned} \tag{4.15}$$

$$\begin{aligned}\beta &= \left(\frac{L}{2}+D\right)\left(\frac{L}{2}-E\right)-F^2\\ &= \frac{1}{4}\left\{L-\sin\left(\frac{2\pi}{L-1}\right)\csc\left(\frac{2\pi}{L(L-1)}\right)\right\}\\ &\quad\times\frac{1}{4}\left\{\cos\left(\frac{2\pi}{L}+2\phi\right)\right\}\\ &\quad\times\left\{L+\sin\left(\frac{2\pi}{L-1}\right)\csc\left(\frac{2\pi}{L(L-1)}\right)\right\}\\ &\quad\times\left\{\cos\left(\frac{2\pi}{L}-2\phi\right)\right\}\\ &\quad-\frac{1}{4}\left\{\sin\left(\frac{2\pi}{L-1}\right)\csc\left(\frac{2\pi}{L(L-1)}\right)\right\}^2\\ &\quad\times\frac{1}{4}\left\{\sin\left(-\frac{2\pi}{L}+2\phi\right)\right\}^2.\end{aligned} \tag{4.16}$$

5 Analysis

5.1 CRB for the Elevation Angle θ

From equations (4.7), (4.12), (4.14) and (4.16)

$$\begin{aligned}
&\frac{\mathrm{CRB}_{\mathrm{UCA}}(\theta)}{\mathrm{CRB}_{\mathrm{UAA}}(\theta)} \\
&= \frac{2\beta}{L\gamma} \\
&= \left\{ \frac{L + \sin\left(\frac{2\pi}{L-1}\right)\csc\left(\frac{2\pi}{L(L-1)}\right)\cos\left(\frac{2\pi}{L} - 2\phi\right)}{L} \right\} \\
&\quad - \frac{\left\{\sin\left(\frac{2\pi}{L-1}\right)\csc\left(\frac{2\pi}{L(L-1)}\right)\sin\left(-\frac{2\pi}{L} + 2\phi\right)\right\}^2}{L\left\{L - \sin\left(\frac{2\pi}{L-1}\right)\csc\left(\frac{2\pi}{L(L-1)}\right)\cos\left(\frac{2\pi}{L} + 2\phi\right)\right\}} \\
&= \frac{L + T_1}{L} - \frac{{T_2}^2}{LT_3}
\end{aligned} \tag{5.1}$$

where,

$$\begin{aligned}
T_1 &= \sin\left(\frac{2\pi}{L-1}\right)\csc\left(\frac{2\pi}{L(L-1)}\right)\cos\left(\frac{2\pi}{L} - 2\phi\right), \\
T_2 &= \sin\left(\frac{2\pi}{L-1}\right)\csc\left(\frac{2\pi}{L(L-1)}\right)\sin\left(-\frac{2\pi}{L} + 2\phi\right), \\
T_3 &= L - \sin\left(\frac{2\pi}{L-1}\right)\csc\left(\frac{2\pi}{L(L-1)}\right)\cos\left(\frac{2\pi}{L} + 2\phi\right).
\end{aligned}$$

5.1.1 When $\frac{\mathrm{CRB}_{\mathrm{UCA}}(\theta)}{\mathrm{CRB}_{\mathrm{UAA}}(\theta)} < 1$

From (5.1) we have

$$\frac{L + T_1}{L} - \frac{{T_2}^2}{LT_3} < 1 \tag{5.2}$$

which implies

$$T_1 T_3 < {T_2}^2. \tag{5.3}$$

This means that UCA has better estimation accuracy as compared to UAA for $L = 4, 5$, $\frac{\pi}{2} \leq \phi \leq \pi$ and $\frac{3}{2}\pi \leq \phi \leq 2\pi$.

5.1.2 When $\frac{\mathrm{CRB}_{\mathrm{UCA}}(\theta)}{\mathrm{CRB}_{\mathrm{UAA}}(\theta)} = 1$

From (5.1) we have

$$\frac{L + T_1}{L} - \frac{{T_2}^2}{LT_3} = 1 \tag{5.4}$$

which implies

$$T_1 T_3 = {T_2}^2. \tag{5.5}$$

This means that UAA and UCA have same performance for $L = 3$ and $0 \leq \phi \leq 2\pi$.

5.1.3 When $\frac{\mathrm{CRB}_{\mathrm{UCA}}(\theta)}{\mathrm{CRB}_{\mathrm{UAA}}(\theta)} > 1$

From (5.1) we have

$$\frac{L + T_1}{L} - \frac{{T_2}^2}{LT_3} > 1 \tag{5.6}$$

which implies

$$T_1 T_3 > {T_2}^2. \tag{5.7}$$

This means that UAA has better estimation accuracy as compared to UCA for $L = 4, 5$, $\frac{\pi}{9} \leq \phi \leq \frac{7}{18}\pi$ and $\frac{10}{9}\pi \leq \phi \leq \frac{25}{18}\pi$.

5.2 CRB for the Azimuth Angle ϕ

From equations (4.8), (4.13), (4.15) and (4.16)

$$\begin{aligned}
&\frac{\mathrm{CRB}_{\mathrm{UCA}}(\phi)}{\mathrm{CRB}_{\mathrm{UAA}}(\phi)} \\
&= \frac{2\beta}{L\alpha} \\
&= \left\{ \frac{L - \sin\left(\frac{2\pi}{L-1}\right) \csc\left(\frac{2\pi}{L(L-1)}\right) \cos\left(\frac{2\pi}{L} + 2\phi\right)}{L} \right\} \\
&\quad - \frac{\left\{ \sin\left(\frac{2\pi}{L-1}\right) \csc\left(\frac{2\pi}{L(L-1)}\right) \sin\left(-\frac{2\pi}{L} + 2\phi\right) \right\}^2}{L\left\{ L + \sin\left(\frac{2\pi}{L-1}\right) \csc\left(\frac{2\pi}{L(L-1)}\right) \cos\left(\frac{2\pi}{L} - 2\phi\right) \right\}} \\
&= \frac{L - T_4}{L} - \frac{{T_2}^2}{LT_5}
\end{aligned} \tag{5.8}$$

where,

$$\begin{aligned}
T_4 &= \sin\left(\frac{2\pi}{L-1}\right) \csc\left(\frac{2\pi}{L(L-1)}\right) \cos\left(\frac{2\pi}{L} + 2\phi\right), \\
T_2 &= \sin\left(\frac{2\pi}{L-1}\right) \csc\left(\frac{2\pi}{L(L-1)}\right) \sin\left(-\frac{2\pi}{L} + 2\phi\right), \\
T_5 &= L + \sin\left(\frac{2\pi}{L-1}\right) \csc\left(\frac{2\pi}{L(L-1)}\right) \cos\left(\frac{2\pi}{L} - 2\phi\right).
\end{aligned}$$

5.2.1 When $\frac{\mathrm{CRB}_{\mathrm{UCA}}(\phi)}{\mathrm{CRB}_{\mathrm{UAA}}(\phi)} < 1$

From (5.8) we have

$$\frac{L - T_4}{L} - \frac{{T_2}^2}{LT_5} < 1 \tag{5.9}$$

which implies

$$-T_4T_5 < {T_2}^2. \tag{5.10}$$

This means that UCA has better estimation accuracy as compared to UAA for $L = 4, 5$, $\frac{\pi}{2} \leq \phi \leq \pi$ and $\frac{3}{2}\pi \leq \phi \leq 2\pi$.

5.2.2 When $\frac{\mathrm{CRB}_{\mathrm{UCA}}(\phi)}{\mathrm{CRB}_{\mathrm{UAA}}(\phi)} = 1$

From (5.8) we have

$$\frac{L - T_4}{L} - \frac{{T_2}^2}{LT_5} = 1 \tag{5.11}$$

which implies

$$-T_4T_5 = {T_2}^2. \tag{5.12}$$

This means that UAA and UCA have same performance for $L = 3$ and $0 \leq \phi \leq 2\pi$.

5.2.3 When $\frac{\mathrm{CRB}_{\mathrm{UCA}}(\phi)}{\mathrm{CRB}_{\mathrm{UAA}}(\phi)} > 1$

From (5.8) we have

$$\frac{L - T_4}{L} - \frac{{T_2}^2}{LT_5} > 1 \tag{5.13}$$

which implies

$$-T_4T_5 > {T_2}^2. \tag{5.14}$$

This means that UAA has better estimation accuracy as compared to UCA for $L = 4, 5$, $\frac{\pi}{9} \leq \phi \leq \frac{7}{18}\pi$ and $\frac{10}{9}\pi \leq \phi \leq \frac{25}{18}\pi$.

6 Numerical Simulations

The following diagrams validates the numerical results in section (5).
Ratios (5.1) and (5.8) are discontinuous when $\csc\left(\frac{2\pi}{L(L-1)}\right) = \infty$ at which points $\sin\left(\frac{2\pi}{L(L-1)}\right) = 0$.

6.1 The Special Cases of $\frac{\mathrm{CRB}_{\mathrm{UCA}}(\theta)}{\mathrm{CRB}_{\mathrm{UAA}}(\theta)}$ and $\frac{\mathrm{CRB}_{\mathrm{UCA}}(\phi)}{\mathrm{CRB}_{\mathrm{UAA}}(\phi)}$

6.1.1 $\frac{\mathrm{CRB}_{\mathrm{UCA}}(\theta)}{\mathrm{CRB}_{\mathrm{UAA}}(\theta)} < 1$ and $\frac{\mathrm{CRB}_{\mathrm{UCA}}(\phi)}{\mathrm{CRB}_{\mathrm{UAA}}(\phi)} < 1$

When $L = 4$ and 5 and $\frac{\pi}{2} \leq \phi \leq \pi$, then from equations (5.1) and (5.8) we obtain Figure 6.1.1.

When $L = 4$ and 5 and $\frac{3}{2}\pi \leq \phi \leq 2\pi$, then from equations (5.1) and (5.8) we obtain Figure 6.1.1. From Figures 6.1.1-6.1.1, it is clear that when $L = 4$ and 5, $\frac{\pi}{2} \leq \phi \leq \pi$ and $\frac{3}{2}\pi \leq \phi \leq 2\pi$, the ratios (5.1) and (5.8) are less than 1.

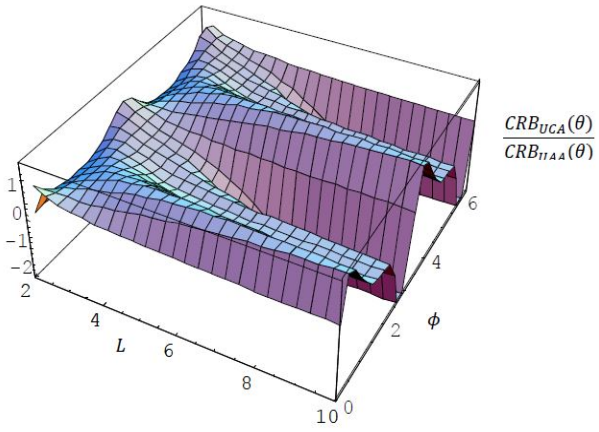

Fig. 3. Comparison of $\mathrm{CRB}_{\mathrm{UCA}}(\theta)$ **and** $\mathrm{CRB}_{\mathrm{UAA}}(\theta)$**.**

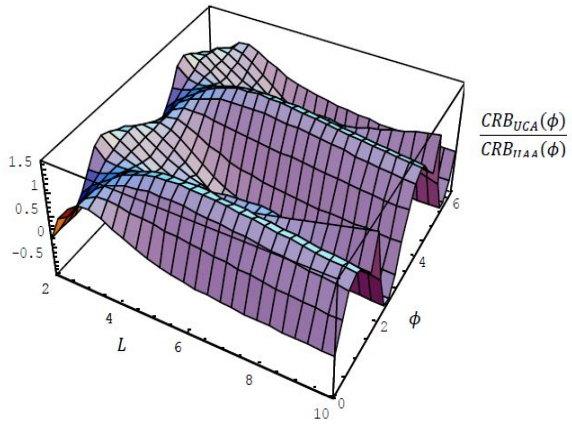

Fig. 4. Comparison of $\mathrm{CRB}_{\mathrm{UCA}}(\phi)$ **and** $\mathrm{CRB}_{\mathrm{UAA}}(\phi)$**.**

6.1.2 $\frac{\mathrm{CRB}_{\mathrm{UCA}}(\theta)}{\mathrm{CRB}_{\mathrm{UAA}}(\theta)} > 1$ and $\frac{\mathrm{CRB}_{\mathrm{UCA}}(\phi)}{\mathrm{CRB}_{\mathrm{UAA}}(\phi)} > 1$

When $L = 4$ and 5 and $\frac{\pi}{9} \leq \phi \leq \frac{7}{18}\pi$, then from equations (5.1) and (5.8) we obtain Figure 6.1.2.

When $L = 4$ and 5 and $\frac{10}{9}\pi \leq \phi \leq \frac{25}{18}\pi$, then from equations (5.1) and (5.8) we obtain Figure 6.1.2. From Figures 6.1.2-6.1.2, it is also clear that when $L = 4$ and 5, $\frac{\pi}{9} \leq \phi \leq \frac{7}{18}\pi$ and $\frac{10}{9}\pi \leq \phi \leq \frac{25}{18}\pi$, the ratios (5.1) and (5.8) are greater than 1.

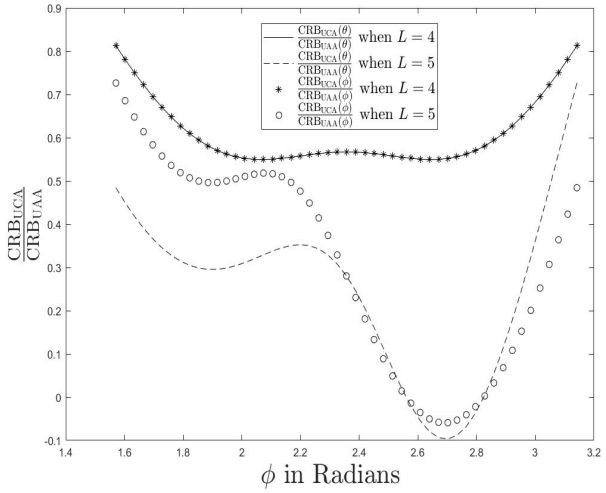

Fig. 5. $\frac{\mathrm{CRB_{UCA}}(\theta)}{\mathrm{CRB_{UAA}}(\theta)} < 1$ **and** $\frac{\mathrm{CRB_{UCA}}(\phi)}{\mathrm{CRB_{UAA}}(\phi)} < 1$ **when** $L = 4$ **and** 5 **and** $\frac{\pi}{2} \leq \phi \leq \pi$

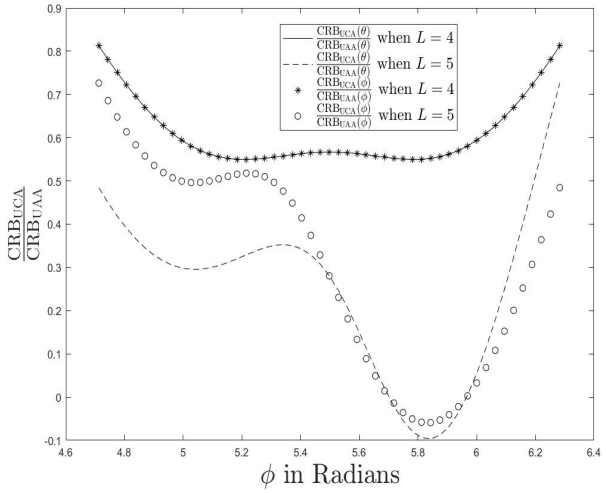

Fig. 6. $\frac{\mathrm{CRB_{UCA}}(\theta)}{\mathrm{CRB_{UAA}}(\theta)} < 1$ **and** $\frac{\mathrm{CRB_{UCA}}(\phi)}{\mathrm{CRB_{UAA}}(\phi)} < 1$ **when** $L = 4$ **and** 5 **and** $\frac{3}{2}\pi \leq \phi \leq 2\pi$

6.1.3 $\frac{\mathrm{CRB_{UCA}}(\theta)}{\mathrm{CRB_{UAA}}(\theta)} = 1$ and $\frac{\mathrm{CRB_{UCA}}(\phi)}{\mathrm{CRB_{UAA}}(\phi)} = 1$

This case was only possible for $L = 3$ and $0 \leq \phi \leq 2\pi$ and therefore from equations (5.1) and (5.8) we obtain Figure 6.1.3. From Figure 6.1.3 it is clear that when $L = 3$ and $0 \leq \phi \leq 2\pi$ for both θ

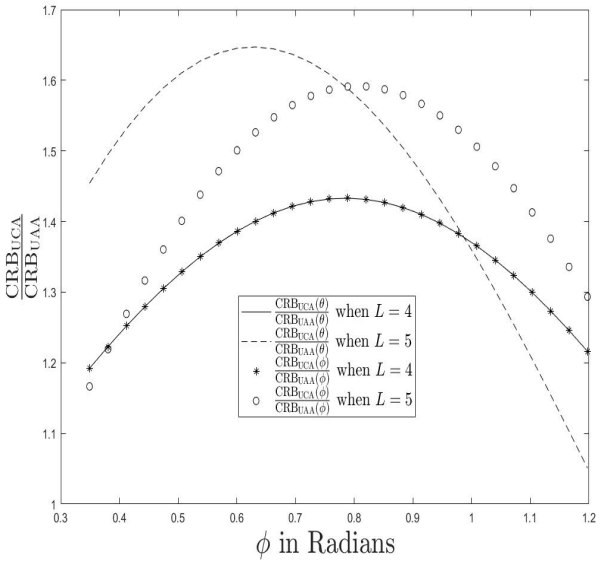

Fig. 7. $\frac{\mathrm{CRB_{UCA}}(\theta)}{\mathrm{CRB_{UAA}}(\theta)} > 1$ **and** $\frac{\mathrm{CRB_{UCA}}(\phi)}{\mathrm{CRB_{UAA}}(\phi)} > 1$ **when** $L = 4$ **and** 5 **and** $\frac{\pi}{9} \leq \phi \leq \frac{7}{18}\pi$

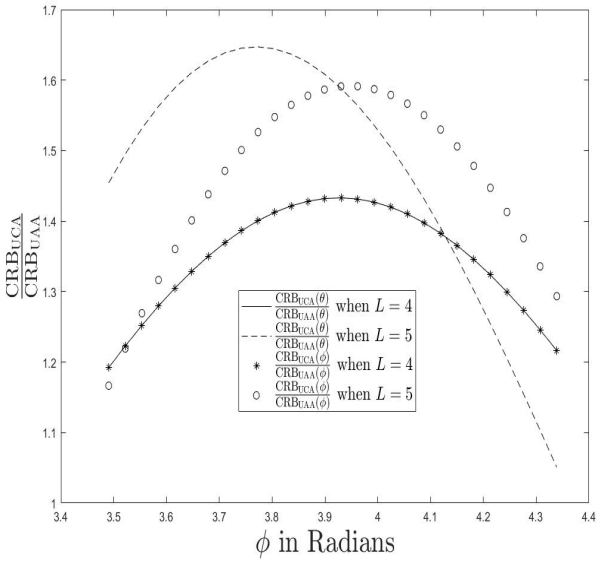

Fig. 8. $\frac{\mathrm{CRB_{UCA}}(\theta)}{\mathrm{CRB_{UAA}}(\theta)} > 1$ **and** $\frac{\mathrm{CRB_{UCA}}(\phi)}{\mathrm{CRB_{UAA}}(\phi)} > 1$ **when** $L = 4$ **and** 5 **and** $\frac{10}{9}\pi \leq \phi \leq \frac{25}{18}\pi$

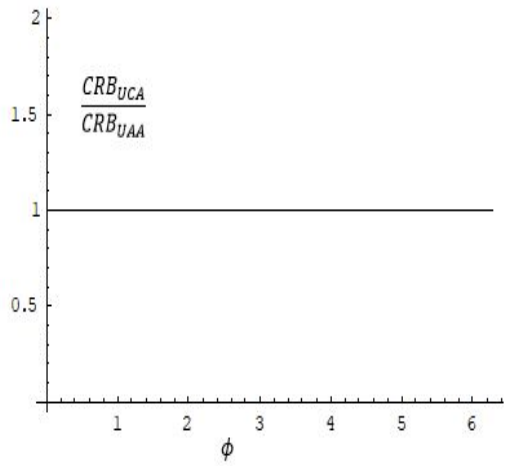

Fig. 9. $\frac{\mathrm{CRB}_{\mathrm{UCA}}(\theta)}{\mathrm{CRB}_{\mathrm{UAA}}(\theta)} = 1$ **and** $\frac{\mathrm{CRB}_{\mathrm{UCA}}(\phi)}{\mathrm{CRB}_{\mathrm{UAA}}(\phi)} = 1$ **when** $L = 3$ **and** $0 \leq \phi \leq 2\pi$

and ϕ, ratios (5.1) and (5.8) are equal to one.

7 Conclusions

The CRBs for both UCA and UAA were derived. Comparison of performance was done by getting the ratio of the obtained CRBs for both elevation angle and azimuth angle. The ratio of the CRB of UCA to the CRB of UAA for both elevation angle and azimuth angle being less than one implied that UCA has better estimation accuracy as compared to UAA.The ratio of the CRB of UCA to that of UAA for both elevation angle and azimuth angle being equals to one implied that UCA and UAA have equal performance. The ratio of the CRB of UCA to that of UAA for both elevation angle and azimuth angle being greater than one implied that UAA has better estimation accuracy as compared to UCA. Therefore, the proposed Uniform Arc Array has better estimation accuracy as compared to Uniform Circular Array when number of sensors equals four and five and azimuth angle ranging between $\frac{\pi}{9}$ and $\frac{7}{18}\pi$ and also $\frac{10}{9}\pi$ and $\frac{25}{18}\pi$. Future studies can focus on better estimation accuracy when the number of sensors increases.

Acknowledgement

The authors are grateful to the referees for their careful reading, constructive criticisms, comments and suggestions, which have helped us to improve this work significantly.

Competing Interests

Authors have declared that no competing interests exist.

References

[1] Manikas A, Sleiman A, Dacos I, Manifold studies of nonlinear antenna array geometries. IEEE Transactions on Signal Processing. 2001;49(3):497-505.

[2] Xiaofei Z, Jianfeng L, Lingyun X, Novel two-dimensional DOA estimation with L-shaped array. EURASIP Journal on Advances in Signal Processing. 2011;1-50.

[3] Tuncer TE, Friedlander B. editors. Classical and modern direction-of-arrival estimation. Academic Press; 2009.

[4] Stoica P, Nehorai A. MUSIC, maximum likelihood, and cramér-rao bound: Further results and comparisons. IEEE Transactions on Acoustics, Speech, and Signal Processing. 1990;38(12)-2140-2150.

[5] Tam PK, Wong KT. Cramér-Rao bounds for direction finding by an acoustic vector sensor under nonideal gain-phase responses, noncollocation, or nonorthogonal orientation. IEEE Sensors Journal. 2009;9(8):969-982.

[6] Kitavi DM, Thomas KW, Chun-Chiu H. An L-shaped array with nonorthogonal axes-its cramér-rao bound for direction finding 2 3 ifa. IEEE Transactions on Aerospace and Electronic Systems. 2017;1-8.

[7] Ciavarrini GM, Greco S, Vecchio A. Geolocation of internet hosts: Accuracy limits through cramér-rao lower bound. Computer Networks; 2018.

[8] Ioannides P, Balanis CA. Uniform circular and rectangular arrays for adaptive beamforming applications. IEEE Antennas and Wireless Propagation Letters. 2005;4(1):351-354.

[9] Tuncer TE, Yasar TK, Friedlander B. Narrowband and wideband doa estimation for uniform and nonuniform linear arrays. 1^{st} ed. Elsevier; 2009.

[10] Tan CM, Fletcher P, Beach M, a R. Nix, Landmann M, Thom RS. On the application of circular arrays in direction finding part I: Investigation into the estimation algorithms. 1st Annual COST 273 Workshop, Espoo, Finland; 2002;29-30.

[11] Shirvani-Moghaddam S, Akbari F. A novel ULA-based geometry for improving AOA estimation. EURASIP Journal on Advances in Signal Processing. 2011;(1)-39.

[12] Wu Y, So HC. Simple and accurate two-dimensional angle estimation for a single source with uniform circular array. IEEE Antennas and Wireless Propagation Letters. 2008;7:78-80.

[13] Kummer WH. Basic array theory. Proceedings of the IEEE. 1992;80(1):127-140.

[14] Lee S, Lo Y. On the pattern function of circular arc arrays. IEEE Transactions on Antennas and Propagaton. 1965;13(4):649-650.

[15] Lim KB, Xin K, Hong GS. Detection and estimation of circular arc segments. Pattern Recognition Letters. 1995;16(6):627-636.

[16] Van HL, Trees. Optimum array processing part IV detection, estimation, and modulation theory. John Wiley and Sons; 2004.

©2019 Nyokabi et al.; This is an Open Access article distributed under the terms of the Creative Commons Attribution License (http://creativecommons.org/licenses/by/4.0), which permits unrestricted use, distribution, and reproduction in any medium, provided the original work is properly cited.

Peer-review history:
The peer review history for this paper can be accessed here (Please copy paste the total link in your browser address bar)
http://www.sdiarticle3.com/review-history/48578